HHS Public Access

Author manuscript

J Clin Neurosci. Author manuscript; available in PMC 2020 June 04.

Published in final edited form as:

J Clin Neurosci. 2019 June ; 64: 214–219. doi:10.1016/j.jocn.2019.03.061.

Directional tuning during reach planning in the supramarginal gyrus using local field potentials

Michael F. Barbaro[a,*], **Daniel R. Kramer**[a], **George Nune**[b], **Morgan B. Lee**[a], **Terrance Peng**[a], **Charles Y. Liu**[a,d], **Spencer Kellis**[a,c,d], **Brian Lee**[a,d]

[a]Department of Neurological Surgery, Keck School of Medicine of USC, University of Southern California, Los Angeles, CA, United States

[b]Department of Neurology, University of Southern California Keck School of Medicine, Los Angeles, CA, United State

[c]Department of Biology and Biological Engineering, California Institute of Technology, Pasadena, CA, United States

[d]USC Neurorestoration Center, Keck School of Medicine of USC, Los Angeles, CA, United States

Abstract

Previous work in directional tuning for brain machine interfaces has primarily relied on algorithm sorted neuronal action potentials in primary motor cortex. However, local field potential has been utilized to show directional tuning in macaque studies, and inferior parietal cortex has shown increased neuronal activity in reaching tasks that relied on MRI imaging. In this study we utilized local field potential recordings from a human subject performing a delayed reach task and show that high frequency band (76–100 Hz) spectral power is directionally tuned to different reaching target locations during an active reach. We also show that during the delay phase of the task, directional tuning is present in areas of the inferior parietal cortex, in particular, the supramarginal gyrus.

Keywords

Local field potential; Directional tuning; Delayed reach; Posterior parietal; Inferior parietal

1. Introduction

Most brain machine interfaces use action potentials as the neuronal feature [1], and decode information from these features to control an assistive device such as a computer or prosthesis. Because the desired machine output often mimics human motion, such as reaching and grasping with a robotic arm, a common substrate for capturing these neural signals is the primary motor cortex. Directional tuning in motor cortex has been shown using

*Corresponding Author at: 1200 North State St., Suite 3300, Los Angeles, CA 90033, United States. mbarbaro@usc.edu (M.F. Barbaro).

5.Competing interests

The authors have no competing interests to declare

neuronal spikes in macaques [2-4]. More recently, spiking activity has found wider use in human subjects [5,6]. Local field potential (LFP) recordings might offer benefits over spike recordings, because LFP signal is more robust to electrode movement (due to a wider field of recording) and tissue scarring [1]. Directional tuning in LFP spectra has been shown in macaques [7].

Research has also shown the presence of directional tuning in regions outside of the primary motor cortex, particularly in the parietal reach region in monkeys [8-10]. Several studies have explored the human analogues to the parietal reach region in the association cortex, using fMRI BOLD signals, and have confirmed that the supramarginal gyrus, the angular gyrus, and regions along the intraparietal sulcus exhibit increased activity when human subjects participate in upper limb reaching tasks and visual saccades [11-14]. Spiking activity in human superior parietal lobule and anterior intraparietal area has been used to control a robotic arm in a tetraplegic subject [6].

In this study, we sought to show the changes in the posterior and inferior parietal lobules during a delayed reach task in a human patient being monitored for epileptiform activity, to confirm the role of these regions in motor planning and execution. Furthermore, we explored whether high frequency (76–100 Hz) LFP spectral power in these regions is biased toward a specific target direction. We show that supramarginal gyrus neural activity, before movement execution, is directionally tuned for the future movement.

2. Methods

Data acquisition.

The subject was a 25 year old left-handed male who used his left hand throughout all trials used in this study. The superior parietal (SP) and inferior parietal (IP) grids seen in Fig. 1c and d were 4 × 5 ECoG grids with 4-mm contacts spaced 10 mm apart from center to center (Integra LifeSciences, Plainsboro, NJ, USA). The 8x8 mini-ECoG grid in the inferior parietal area (MP) used 2-mm contacts with 3-mm spacing (FG64C-MP03, Ad-Tech Medical Instrumentation Corporation, Oak Creek, WI, USA). All neural activity was amplified, digitized, and recorded (Neuroport System, Blackrock Microsystems, Salt Lake City, UT, USA) in the neurosurgical ICU during phase II monitoring of epileptiform activity. Electric potentials were sampled from these electrodes at 2000 samples/sec.

Experiment.

The experimental task was programmed in MATLAB (The Mathworks) with the Psychophysics Toolbox. Task visuals were displayed on a touchscreen monitor within arm's reach of the subject. The task consisted of 5 phases (Fig. 1a and b): after an inter-trial interval (2 s), the research participant was instructed to fix their gaze on a grey circle presented at the center of the screen (2 s). Next, one of eight radial target locations was presented as a white circle in a cue phase (1 s), and, following a brief delay (1 s) in which the target was removed but the fixation point remained, the fixation point disappeared and the subject reached out to touch the monitor screen at the cued (remembered) location. Target locations were distributed across trials in a pseudorandom, uniform order, eight times

for each target location for a total of 64 trials in each task. Touch locations and time were recorded, and each trial was counted successful if the touch location was within 2 radii of the target center.

Signal Processing.

Raw neural signal was visually inspected and electrodes with excessive noise were excluded from analysis. Each grid was processed separately due to structural differences and spatial separation. A common average reference was applied to the raw signal before performing spectral analysis. The Chronux package was used to compute multi-tapered spectrograms [15], with a window size of 250 ms, step size of 100 ms, frequency range of 0–500 Hz, each window zero-padded to 1024 points. The timebandwidth parameter was set to 3 and the number of tapers was 5. Spectrograms were computed for each phase of each trial for each channel, and the trial average was computed for a channel's spectrum in a given phase (Fig. 2b).

Activations.

Spectral power changes were compared in the Delay and Response phases, in a low frequency band (8–32 Hz) and a high frequency band (76–100 Hz). The Cue phase was used as a baseline for these comparisons so that visual confounds would cancel when referenced against the phase of interest. To quantify these comparisons, we computed an "activation" index [16,17] for each channel, frequency band, and phase of interest. Activation is a signed comparison of means, scaled by the variance and the number of trials. We first calculated the variance r of spectrogram power across all trials, along with the average power x in each phase, the average power c in the Cue phase, and the number of trials in the phase of interest N_x, the cue phase N_c, and the total number of trials N_{xc}, and then computed the activation:

$$Activation = \frac{(x-c)^3}{|x-c|\sigma^2} \cdot \frac{N_x N_c}{N_{xc}}$$

Statistical significance of the activations was computed by comparing measured values to a null distribution, created by randomly sorted the data into two groups to compute new activation values and repeating 10,000 times. The measured activation value was deemed significant if it was greater in magnitude than 95% of the bootstrapped distribution. Significant values were used as inputs to a two-dimensional Gaussian-smoothed heat map plotted by color over the spatial extent of the electrodes (e.g. Fig. 2a).

Tuning.

The activation values for each target were calculated as described above, but for data sorted and averaged by target location. We focused on the high frequency band to assess directional tuning given its typical correlation to multiunit recordings [18]. Values that exceeded 1.5 times the interquartile range of the target activations were excluded as outliers. After shifting the activation values circularly to center the maximum value, and subtracting the minimum activation value so that the ‘‘tuning curve" rested on the line y = 0, a Gaussian curve was fit to the activation values and goodness-of-fit assessed with the coefficient of determination

(r^2) [7,8]. Significance was established if the r^2 values were larger than 95% of r^2 values generated from a Gaussian fit of 10,000 shuffled samples of a channel's trials.

Figures. 3-D reconstructions of ECoG grid locations were created using the img_pipe package [19]. Pre-operative T1 magnetic resonance imaging (MRI) scans were merged with post-operative computed tomography (CT) scans containing the electrode locations. Co-registration was performed using Statistical Parametric Mapping software SPM12 [20]. 3-D pial surface reconstructions were created from the pre-operative MRI sequence using Freesurfer [21].

3. Results

The different phases of the experimental task can be seen in Fig. 1a and the potential target locations in Fig. 1b. Grid coverage can be seen in Fig. 1c, d with the superior parietal (SP) grid covering areas of motor and sensory cortex, along with part of the intraparietal sulcus. The mini-grid in the parietal region (MP) spans the termination of the lateral sulcus, part of the supramarginal gyrus and inferior parietal lobule. The most posterior grid is in the inferior parietal (IP) lobe as well and covers the angular gyrus and posterior end of the intraparietal sulcus.

Spectral power differences when moving, previously seen in experiments involving the motor cortex [16], were observed in association cortex. The motor cortex region covered by the SP grid exhibits the expected high frequency band power increase and low frequency power decrease in the response phase compared to the cue (Fig. 2b top left). Interestingly, electrodes on the MP grid, covering the supramarginal gyrus, also exhibit the same pattern of activation during the reaching phase (Fig. 2b top right), along with electrode 10 of the SP grid located over posterior parietal cortex. There were also regions in the posterior and inferior parietal cortex where high frequency band power increased, and low frequency band power decreased, but during the delay phase. A region of the MP grid on the anterior border of the lateral sulcus also showed increased high frequency power, while a more widespread region exhibited decreased low frequency power in the delay phase. In contrast, the motor region (SP grid) had no difference in spectral power during the delay phase (Fig. 2b bottom left).

To investigate the time course of changes in the activation values, activations were calculated in the high frequency band for each of the overlapping spectrogram time windows during the delay phase and response phase for all targets. Electrodes with significant activations were plotted in a Gaussian-smoothed heat map as seen in Fig. 3. Increased high frequency band activation is seen early in the delay phase in the lower supramarginal gyrus, which then attenuates before migrating in a superior and anterior direction. No significant high frequency activation is seen in the superior parietal region during the delay period, while a high frequency activation decrease is seen in the inferior portion of the IP grid. This region of decreased activation continues into the response phase. Subsequently, the activation in the anterior supramarginal gyrus increases, along with an activation increase in the superior parietal region consistent with motor cortex activity during a reaching movement. There is

also increased high frequency activation in a posterior, superior parietal area, near the intraparietal sulcus.

To further investigate the directional tuning of these areas, we calculated the activation of the target-averaged spectral power for each channel in the high frequency band. Tuning curves in the delay and response phases, along with polar plots of both phases' target-specific activation values, can be seen for representative channels in Fig. 4. Channel 2 of the SP grid had significant ($p = 0.048$) tuning in the response phase, with a similarly directed but insignificant tuning in the delay phase ($p = 0.136$) (Fig. 4a). Fig. 4b, c show SP channel 15 and MP channel 29, respectively, which both exhibit significant directional tuning in the delay phase.

4. Discussion

This study provides new insight into activity in human inferior parietal cortex during planning and executing a reaching movement. It shows that LFP changes in high and low frequency bands typically seen in primary motor cortex are also seen in parts of the supramarginal gyrus during reaching. These findings are consistent with those previously seen in macaque studies [22] and with reaching tasks in humans utilizing fMRI [23], shown here using ECoG grids in humans.

Previous work has shown that kinematic parameters can be decoded from primary motor cortex LFP signals in monkeys [7,18,24], as well as humans [25]. These studies found significant movement tuning using high frequency (>60 Hz) spectral power, in a similar fashion to our work. High gamma spectral power may reflect multiunit neural activity, and research has shown that kinematic parameters in high frequency LFP spectra correlate with multiunit recordings more strongly than low frequency spectra [18,26]. We likewise postulate that the directional tuning found in posterior and inferior parietal locations reflects multiunit activity that increases signaling activity during the planning phase of a movement. Incorporating activity from these areas in a braincomputer interface may lead to better control, as movement intentions may be cognitively more natural to exercise than attempted physical movement for tetraplegic persons [6]. Future work will be directed towards analyzing whether target location can be accurately predicted from neural activity in the inferior parietal cortex.

Different regions covered by the MP grid also showed increased high frequency activation with decreased low frequency activation, but during the Delay phase only. This data agrees with fMRI studies showing increased activity in the right inferior parietal lobule during the delay phase of a grasping task [27,28]. Studies involving electrical stimulation of the human inferior parietal lobule elicited a "desire to move" [29,30]. This raises the question of whether increased neural activity in this region is associated with planning a subsequent movement, or with an intent to move in a general sense. By showing that channels are directionally tuned to the reach location during the Delay phase, this finding suggests that those locations are associated with planning the reach. However, other research has suggested that neurons in these locations may serve both functions [10], which highlights the need for further experimental analysis.

We also acknowledge the difficulty in extrapolating significance from these results with data from only one subject. While we hope to replicate these findings with future subjects, the location for implanted ECoG arrays is ultimately decided by the clinical need of the patient.

References

[1]. Hwang EJ, Andersen RA. The utility of multichannel local field potentials for brain-machine interfaces. J Neural Eng 2013;10:046005. [PubMed: 23744624]

[2]. Amirikian B, Georgopoulos AP. Directional tuning profiles of motor cortical cells. Neurosci Res 2000;36:73–9. [PubMed: 10678534]

[3]. Georgopoulos AP, Kalaska JF, Caminiti R, Massey JT. On the relations between the direction of two-dimensional arm movements and cell discharge in primate motor cortex. J Neurosci 1982;2:1527–37. [PubMed: 7143039]

[4]. Baker J, Bishop W, Kellis S, Levy T, House P, Greger B. Multi-scale recordings for neuroprosthetic control of finger movements. Conf Proc IEEE Eng Med Biol Soc 2009;2009:4573–7. [PubMed: 19963841]

[5]. Wodlinger B, Downey JE, Tyler-Kabara EC, Schwartz AB, Boninger ML, Collinger JL. Ten-dimensional anthropomorphic arm control in a human brain-machine interface: difficulties, solutions, and limitations. J Neural Eng 2015;12:016011. [PubMed: 25514320]

[6]. Aflalo T, Kellis S, Klaes C, Lee B, Shi Y, Pejsa K, et al. Decoding motor imagery from the posterior parietal cortex of a tetraplegic human. Science 2015;348:906–10. [PubMed: 25999506]

[7]. Rickert J, Oliveira SC, Vaadia E, Aertsen A, Rotter S, Mehring C. Encoding of movement direction in different frequency ranges of motor cortical local field potentials. J Neurosci 2005;25:8815–24. [PubMed: 16192371]

[8]. Scherberger H, Jarvis MR, Andersen RA. Cortical local field potential encodes movement intentions in the posterior parietal cortex. Neuron 2005;46:347–54. [PubMed: 15848811]

[9]. Snyder LH, Batista AP, Andersen RA. Coding of intention in the posterior parietal cortex. Nature 1997;386:167–70. [PubMed: 9062187]

[10]. Calton JL, Dickinson AR, Snyder LH. Non-spatial, motor-specific activation in posterior parietal cortex. Nat Neurosci 2002;5:580–8. [PubMed: 12021766]

[11]. Astafiev SV, Shulman GL, Stanley CM, Snyder AZ, Van Essen DC, Corbetta M. Functional organization of human intraparietal and frontal cortex for attending, looking, and pointing. J Neurosci 2003;23:4689–99. [PubMed: 12805308]

[12]. Shulman GL, McAvoy MP, Cowan MC, Astafiev SV, Tansy AP, d'Avossa G, et al. Quantitative analysis of attention and detection signals during visual search. J Neurophysiol 2003;90:3384–97. [PubMed: 12917383]

[13]. Koyama M, Hasegawa I, Osada T, Adachi Y, Nakahara K, Miyashita Y. Functional magnetic resonance imaging of macaque monkeys performing visually guided saccade tasks: comparison of cortical eye fields with humans. Neuron 2004;41:795–807. [PubMed: 15003178]

[14]. Connolly JD, Andersen RA, Goodale MA. FMRI evidence for a 'parietal reach region' in the human brain. Exp Brain Res 2003;153:140–5. [PubMed: 12955383]

[15]. Bokil H, Andrews P, Kulkarni JE, Mehta S, Mitra PP. Chronux: a platform for analyzing neural signals. J Neurosci Methods 2010;192:146–51. [PubMed: 20637804]

[16]. Miller KJ, Leuthardt EC, Schalk G, Rao RP, Anderson NR, Moran DW, et al. Spectral changes in cortical surface potentials during motor movement. J Neurosci 2007;27:2424–32. [PubMed: 17329441]

[17]. Miller KJ, Zanos S, Fetz EE, den Nijs M, Ojemann JG. Decoupling the cortical power spectrum reveals real-time representation of individual finger movements in humans. J Neurosci 2009;29:3132–7. [PubMed: 19279250]

[18]. Liu J, Newsome WT. Local field potential in cortical area MT: stimulus tuning and behavioral correlations. J Neurosci 2006;26:7779–90. [PubMed: 16870724]

[19]. Hamilton LS, Chang DL, Lee MB, Chang EF. Semi-automated anatomical labeling and inter-subject warping of high-density intracranial recording electrodes in electrocorticography. Front Neuroinform 2017;11:62. [PubMed: 29163118]

[20]. Ashburner J, Friston K. Multimodal image coregistration and partitioning–a unified framework. Neuroimage 1997;6:209–17. [PubMed: 9344825]

[21]. Fischl B FreeSurfer. Neuroimage 2012;62:774–81. [PubMed: 22248573]

[22]. Chang SW, Snyder LH. Idiosyncratic and systematic aspects of spatial representations in the macaque parietal cortex. Proc Natl Acad Sci U.S.A. 2010;107:7951–6. [PubMed: 20375282]

[23]. Filimon F, Nelson JD, Huang RS, Sereno MI. Multiple parietal reach regions in humans: cortical representations for visual and proprioceptive feedback during on-line reaching. J Neurosci 2009;29:2961–71. [PubMed: 19261891]

[24]. Perel S, Sadtler PT, Godlove JM, Ryu SI, Wang W, Batista AP, et al. Direction and speed tuning of motor-cortex multi-unit activity and local field potentials during reaching movements. Conf Proc IEEE Eng Med Biol Soc 2013;2013:299–302. [PubMed: 24109683]

[25]. Schalk G, Kubanek J, Miller KJ, Anderson NR, Leuthardt EC, Ojemann JG, et al. Decoding two-dimensional movement trajectories using electrocorticographic signals in humans. J Neural Eng 2007;4:264–75. [PubMed: 17873429]

[26]. Zhuang J, Truccolo W, Vargas-Irwin C, Donoghue JP. Decoding 3-D reach and grasp kinematics from high-frequency local field potentials in primate primary motor cortex. IEEE Trans Biomed Eng 2010;57:1774–84. [PubMed: 20403782]

[27]. Fiehler K, Bannert MM, Bischoff M, Blecker C, Stark R, Vaitl D, et al. Working memory maintenance of grasp-target information in the human posterior parietal cortex. Neuroimage 2011;54:2401–11. [PubMed: 20932912]

[28]. Bernier PM, Grafton ST. Human posterior parietal cortex flexibly determines reference frames for reaching based on sensory context. Neuron 2010;68:776–88. [PubMed: 21092865]

[29]. Desmurget M, Reilly KT, Richard N, Szathmari A, Mottolese C, Sirigu A. Movement intention after parietal cortex stimulation in humans. Science 2009;324:811–3. [PubMed: 19423830]

[30]. Desmurget M, Sirigu A. Conscious motor intention emerges in the inferior parietal lobule. Curr Opin Neurobiol 2012;22:1004–11. [PubMed: 22939569]

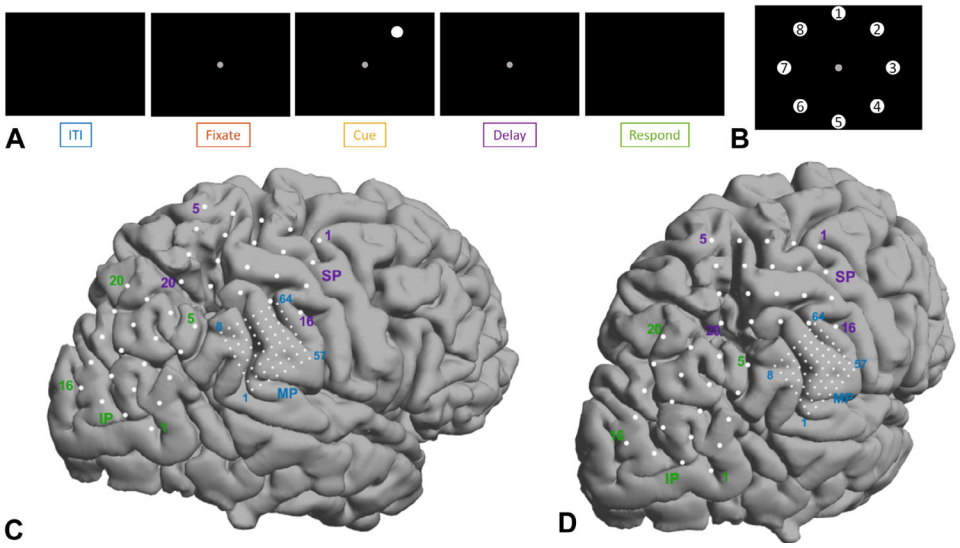

Fig. 1.

A) The experimental task, showing the five separate phases. Following the intertrial interval (ITI), a central fixation point was shown. The cue was presented from one of eight target locations, which was then removed for the delay period. The subject was indicated to reach and touch the remembered target location after the fixation point was removed. Colors of phase names are used in subsequent figures. B) The eight radial target locations, each presented a total of eight times throughout the task. C) Lateral view of grid locations and orientation on the right hemisphere of S1. SP: superior parietal, MP: mini-parietal, IP: inferior parietal. D) Posteriorly rotated view of grid locations.

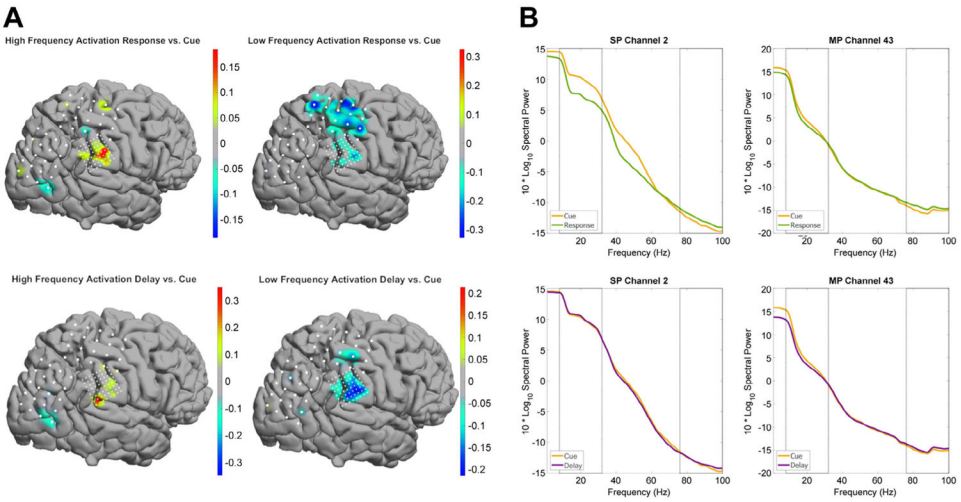

Fig. 2.

A and B. A) Differences in spectral power are represented by activation heat maps shown on the left (high frequency left, low frequency right) which are scaled to the maximum absolute activation value. Activation values for the response phase (top row) and delay phase (bottom row). B) Spectra from 2 representative channels from the superior parietal (SP) grid (left column) and the mini parietal (MP) grid (right column) showing increased low frequency power (8–32 Hz) for the cue phase (yellow) compared to the response phase (green), but increased high frequency power (76–100 Hz) for the response phase compared to the cue (top row). For the delay phase compared to cue (bottom row), the same SP channel shows minimal differences in power between phases, but the representative channel from MP shows decreased low frequency power and increased high frequency power.

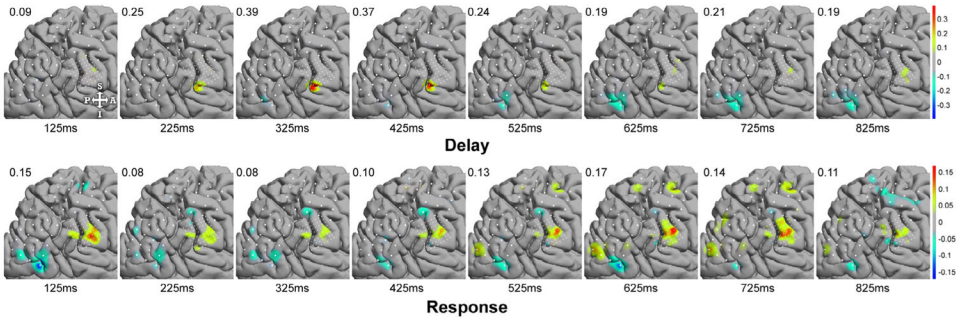

Fig. 3.

High frequency activation for each time-step of the spectrogram sliding window. Top: the Delay phase shows increased activation in a focal region of the inferior parietal lobule that migrates anteriorly and stays elevated during the Response phase. A channel in the superior parietal grid overlying primary motor cortex also increased in activation during this phase. The value in each frame represents the largest in magnitude activation value for all grids pictured. Time stamps on the x-axis represent the midpoint of each time window pictured. Numbers in the top left of each frame represent the largest magnitude activation value from that frame.

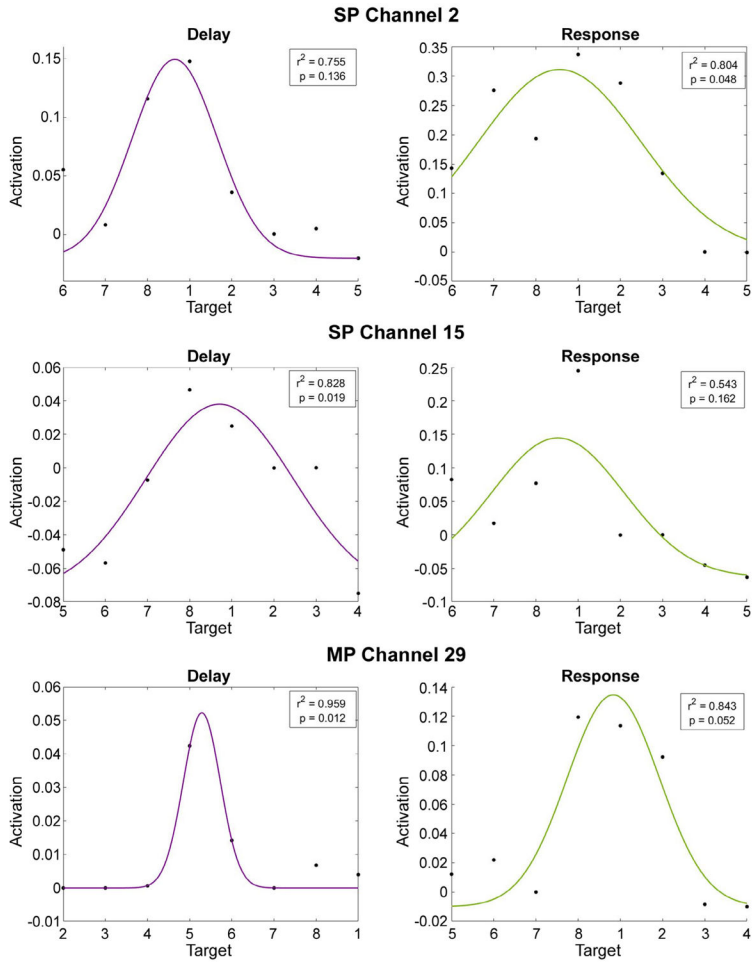

Fig. 4.

The left column represents Delay phase activation, and the right column represents Response phase activations. Left and Right columns contain 76–100 Hz activations from target averaged spectral power, with targets numbers on the x-axis shifted to centralize maximum activations. R^2 values are top-right, along with p-values calculated from bootstrap reshuffled target values. Tuning curves with significant R^2 values are boxed. A) SP channel 2, showing significant tuning during the response phase. B) SP channel 15, located in a superior posterior parietal region, with significant tuning during the delay phase, but not the response phase. C) MP channel 29, located in superior marginal gyrus, with significant tuning in the delay phase.